# Nanoscale

Accepted Manuscript


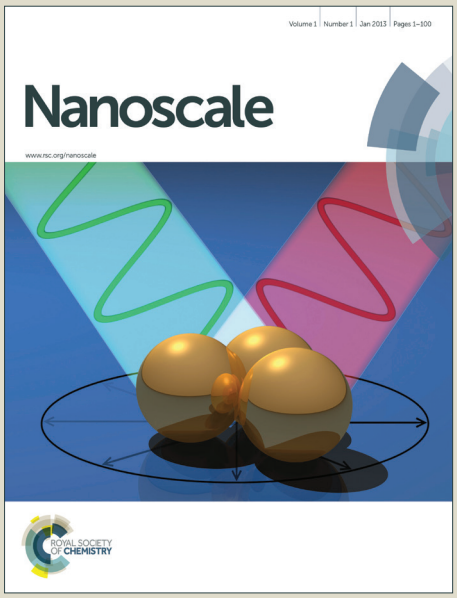

Journal Name

ARTICLE

# Two-dimensional Nanosheets of $MoS_2$: A Promising Material with High Dielectric Properties and Microwave Absorption Performances

Received 00th January 20xx,
Accepted 00th January 20xx

DOI: 10.1039/x0xx00000x

www.rsc.org/

Ming-Qiang Ning,‡ Ming-Ming Lu,‡ Jing-Bo Li,* Zhuo Chen, Yan-Kun Dou, Cheng-Zhi Wang, Fida Rehman, Mao-Sheng Cao,* Hai-Bo Jin*

In this work, few-layer $MoS_2$ nanosheets ($MoS_2$-NS) were obtained via the top-down exfoliation method from bulk $MoS_2$ ($MoS_2$-Bulk), and the dielectric properties and microwave absorption performances of $MoS_2$-NS were first reported. Dimension-dependent dielectric properties and microwave absorption performances of $MoS_2$ were investigated by presenting a comparative study between $MoS_2$-NS and $MoS_2$-Bulk. Our results show that the imaginary permittivity ($\varepsilon''$) of the $MoS_2$-NS/wax is twice as large as that of the $MoS_2$-Bulk/wax . The minimum reflection loss (RL) value of $MoS_2$-NS/wax with 60 Wt.% loading is -38.42 dB at the thickness of 2.4 mm which is almost 4 times higher than that of MoS2-Bulk/wax, and the corresponding bandwidth with effective attenuation (< -10 dB) of $MoS_2$-NS/wax is up to 4.1 GHz (9.6-13.76 GHz ). The microwave absorption performance of $MoS_2$-NS is comparable to those reported in carbon related nanomaterials. The enhanced microwave absorption performance of $MoS_2$-NS is attributed to the defect dipole polarization arising from Mo and S vacancies and its higher specific surface area. These results suggest that the $MoS_2$-NS is not only a promising candidate material in fundamental studies but also in practical microwave application.

## 1.Introduction

Searching for lightweight, high-efficiency, wide-absorption frequency ranges and low-cost industrial processing has been actively pursued owing to its importance in the practical applications of electromagnetic (EM) wave absorbing materials.[1-10] Based on the above requirements, carbon nanomaterials included carbon nanosheets (CNSs),[11] carbon nanotubes (CNTs), [10,12] carbon nanocoils (CNCs) [4,13] and carbon nanofibers (CNFs)[14] have received significant investigation in the field of microwave absorption for their outstanding physicochemical properties and corresponding dimension structure. As an excellent representative of the carbon material, the reduced graphene oxides (R-GO), the thinnest and most lightweight 2D materials of the carbon world, have been also reported to exhibit excellent dielectric properties because of its higher specific surface area and clustered defects.[15]Actually, 2D materials such as graphene,[16-18] hexagonal boron nitride (h-BN), [19,20] carbon nitride ($C_3N_4$)[21-23]and and layer transition metal dichalcogenides (LTMD) [24-26] have also shown their substantial application potential in optoelectronics, biomedicine, catalysis and so on. These can be attributed to their exotic electronic properties caused by the strictly defined dimensionalities, high specific surface areas and polymorphism which are the three main unique features of 2D materials. [27-29] As a widely known LTMD, molybdenum disulfide ($MoS_2$), which consists of S-Mo-S triple layers bound by weak van der Waals forces, has increasingly attracted much attention recently since they exhibit unique electrical, optical and mechanical properties with respect to its bulk counterparts. Recent reports in the field of photoluminescence,[30,31] hydrogen evolution[32-34] and biomedical applications of $MoS_2$ nanosheets have opened up new prospects for realization of novel nanodevices with

*School of Material Science and Engineering, Beijing Institute of Technology, Beijing 100081, China. E-mail: hbjin@bit.edu.cn, lijb@bit.edu.cn, caomaosheng@bit.edu.cn*
† Electronic Supplementary Information (ESI) available: Fig S1-5 and Table S1. See DOI: 10.1039/x0xx00000x
‡Ming-Qiang Ning, Ming-Ming Lu contributed equally to this work

advanced functionalities. However, compared with the intensive study of graphene, there is absent of a detailed investigation of the dielectric properties and microwave absorption performances of $MoS_2$-NS. In general, solution based exfoliation methods are usually used to obtain large quantities of mono- or few-layers $MoS_2$ sheets[35,36] and those methods could give rise to new and interesting properties. Besides the higher specific surface area, a very intriguing phenomenon is that there is a phase transition from trigonal prismatic (2H-$MoS_2$) semiconducting phase to octahedral (1T-$MoS_2$) metallic phase. [37-39] Moreover, $MoS_2$-NS may contain much more surface defects including S vacancies (Vs), Mo vacancies ($V_{Mo}$) due to the violent exfoliation process compared to $MoS_2$-Bulk and those defects would have great effects on $MoS_2$-NS's electronic properties.[40-42] All these attributes suggest that the $MoS_2$-NS has a great potential in microwave absorption applications. Inspired by the excellent microwave absorption performances exhibited by recent work on graphene-related materials and combined with the intriguing properties of $MoS_2$-NS, we focus on the dielectric properties and microwave absorption performances of $MoS_2$-NS. In this work, we prepared $MoS_2$-NS samples by top-down exfoliation method, demonstrated the excellent microwave absorption performances of $MoS_2$-NS and discussed possible mechanism of enhanced microwave absorption performance of $MoS_2$-NS. To the best of our knowledge, this is the first systematical report about dielectric properties and microwave absorption performances of $MoS_2$-NS.

## 2. Experimental section

### 2.1 Materials

The commercial $MoS_2$ powder was purchased from Aladdin. Hexane, N-butyl lithium (1.6M in hexanes), anhydrous ethanol, deionized water and ether were supplied by Beijing Chemical Corporation. All reagents were analytical grade and used as received.

### 2.2 Preparation of samples

#### Preparation of $MoS_2$-NS samples and annealed $MoS_2$-NS samples

$MoS_2$-NS were obtained via the Per Joensen's method. [36] The exfoliation process is shown in Fig 1(a) which involves two steps. The first step is to intercalate the $MoS_2$: 100 mg of the commercial $MoS_2$ powder was soaked in 10 mL of n-butyl lithium for 5 days at room temperature. Then, excess n-butyl lithium was removed by washing the samples for several times with hexane. The above step was completed in an argon-filled glove box. The second step, exfoliation process is as follows: the intercalated samples were exfoliated with distilled water in a vial by using ultrasound-assisted. The obtained suspension was centrifuged, dried at 60 ℃ under vacuum. Finally, the solid product $MoS_2$-NS were collected for further experiments. For comparison, the annealed $MoS_2$-NS samples were prepared by heating the $MoS_2$-NS samples at 150℃ for 3h.

#### Preparation of $MoS_2$-Bulk/wax, $MoS_2$-NS/wax and the annealed $MoS_2$-NS/wax

In the dielectric measurement as shown in FigS1, the specific quantity of $MoS_2$ materials ($MoS_2$-Bulk, $MoS_2$-NS and annealed $MoS_2$-NS: 30, 40, 50 and 60 Wt.%) and paraffin wax (70, 60, 50 and 40 Wt.%) were added to a vial containing appropriate amount of ether and then ultrasonic treatment for one hour. The $MoS_2$ materials/wax were cooled to room temperature after the ether solution evaporated completely and pressed into a test sample (outer radius: 7.00mm; inner radius: 3.00mm).[43]

### 2.3 Characterization

Powder X-ray diffraction (XRD) patterns were collected on a Bruker-AXS diffractometer (Model D8 ANVANCE) with Cu-$K\alpha$ radiation source. Atomic force microscope (AFM) images were obtained on a Veeco Dimension Fast Scan system. Scanning electron microscope (SEM) images were obtained by a Hitachi S-480. Transmission electron microscope (TEM) images were obtained by a FEI Tecnai G2 F20S-TWIN. The thermal stability of samples was measured by DSC-TGA (NETZSCH DSC 204 F1 Phoenix, NETZSCH TG 209 F1) under air

atmosphere with a heating rate of 1 ℃ $min^{-1}$. Raman Spectroscopy measurements were performed on Lab RAM Aramis. X-ray photoelectron spectroscopy (XPS) was measured on a PHI Quantera system with a C60 ion gun. Keithley 4200-SCS semiconductor characterization system was used to measure the conductivity of the samples. The relative permittivity was measured at 2-18 GHz on the Anritsu 37269D vector network analyzer by the coaxial method.

## 3. Results and discussion

### 3.1 Morphology, structure and phase

The SEM images of $MoS_2$-Bulk and $MoS_2$-NS are shown in Fig.1 b-e. Much smaller and uniform $MoS_2$-NS (marked by red circle) were obtained as shown in Figure 1(d-e).

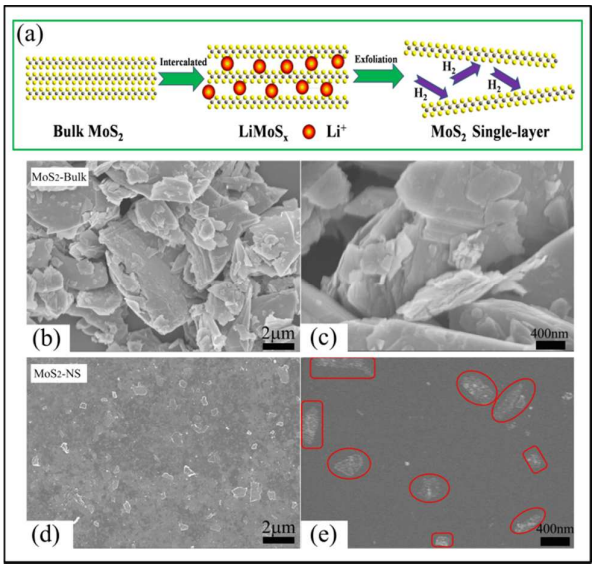


Fig.1 (a): Illustration of the exfoliation method for achieving $MoS_2$-NS. (b-c) SEM images of $MoS_2$-Bulk. (d-e) SEM images of $MoS_2$-NS.

Figure 2(a) shows the TEM image of well transparent $MoS_2$-NS. The TEM image suggests that the $MoS_2$-NS is flexible and quite thin. A close observation to the surface by TEM image reveals that the $MoS_2$-NS are few-layered or even monolayer. The selected area electron diffraction (SAED) indicates the fact $MoS_2$-NS are well crystallized. The AFM image (Fig 2b) shows that the obtained $MoS_2$-NS are typically less than 2.5 nm in thickness and 0.1~0.5 μm in extent. Fig 2 (c) shows the XRD pattern of $MoS_2$-NS and $MoS_2$-Bulk samples. The diffraction peaks of $MoS_2$-Bulk are well indexed to 2H-$MoS_2$ (PDF# 37-1492). For $MoS_2$-NS samples, the wide diffraction peaks imply the nano-size nature of the samples, and the pattern is in good agreement with that of the few-layer $MoS_2$.[36]

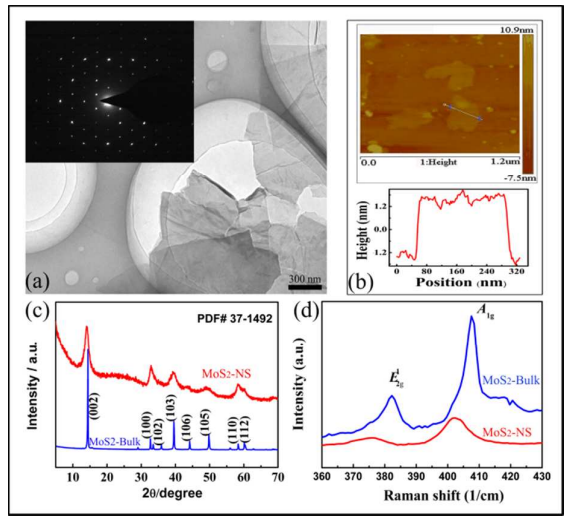


Fig .2 (a) TEM (Inset: SAED of $MoS_2$-NS samples) and (b) AFM image of $MoS_2$-NS and the corresponding height profile. (c) XRD and (d) Raman spectra of $MoS_2$-Bulk and $MoS_2$-NS samples.

Raman spectra can be used to evidence the acquisition of few-layer nano-thin $MoS_2$ from the peak frequency difference (Δω) between the in-plane vibrational mode ($E^1_{2g}$) and the out-of-plane vibrational mode ($A_{1g}$). For the Raman spectra of $MoS_2$-Bulk shown in Fig 2 (d), the strong $E^1_{2g}$ mode at ~381 $cm^{-1}$ and the $A_{1g}$ mode ~409 $cm^{-1}$ are in good agreement with those reported in bulk $MoS_2$.[44] However, both $A_{1g}$ and $E^1_{2g}$ modes of $MoS_2$-NS are clearly softened and blue shift compared to $MoS_2$-Bulk. It is consistent with the previous results reported by C. N. R. Rao et al and the corresponding bands at 378 $cm^{-1}$ and 402 $cm^{-1}$ are considered to be due to phonon confinement.[45] Lee et al. have managed to identify the layer number of $MoS_2$-NS depending on the Δω between $A_{1g}$ and $E^1_{2g}$ modes.[44] In this work, the Δω between $A_{1g}$ and $E^1_{2g}$ modes of $MoS_2$-NS samples is ~24 $cm^{-1}$, from which the layer number of $MoS_2$-NS is deduced to be about 3~4. That corresponds to ~2.6 nm in thickness (calculated with ~0.65 nm for each monolayer). The thickness of ~2.6 nm is coincident with the results of AFM analysis in front.

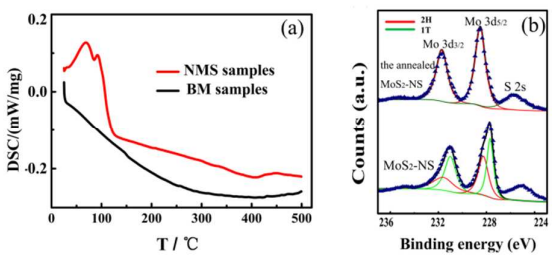


Fig.3 (a) DSC of $MoS_2$-Bulk and $MoS_2$-NS samples. (b) XPS spectra showing Mo 3d peak regions of $MoS_2$-NS sample and the annealed $MoS_2$-NS sample.

As mentioned above, there is a phase transition from 2H to 1T during the exfoliation process, consequently the obtained $MoS_2$-NS samples could be mixed-phase. However, the 1T phase is not stable, and can transforms back to the 2H phase under moderate-temperature annealing. The mixed phase nature of prepared $MoS_2$-NS samples is evidenced by DSC and XPS measurements. Fig.3 (a) shows the DSC results of $MoS_2$-NS and $MoS_2$-Bulk samples. The exothermic peak of $MoS_2$-NS around 95℃ indicates the irreversible phase transition from 1T to 2H and is consistent with the transiton temperature reported in Wypych's work.[46] Figure 3 (b) shows the XPS results of $MoS_2$-NS and annealed $MoS_2$-NS samples. The annealed $MoS_2$-NS samples are undoubtedly proved to be 2H-phase by showing the Mo $3d_{5/2}$ and Mo $3d_{3/2}$ orbitals at 228.5 and 231.8eV and the S $2p_{1/2}$ at 162.5eV, S $2p_{3/2}$ at 161.4eV. As for $MoS_2$-NS, the apparent red shift was observed and the additional peaks found at 228.1 eV (green line of Mo $3d_{5/2}$), 231.3 eV (green line of Mo $3d_{3/2}$) are considered to be 1T phase according to previous similar results.[31,47] Similarly, the additional peaks found in S 2p spectra arise from 1T phase as shown in Figure S2.

## 3.2. Dielectric properties

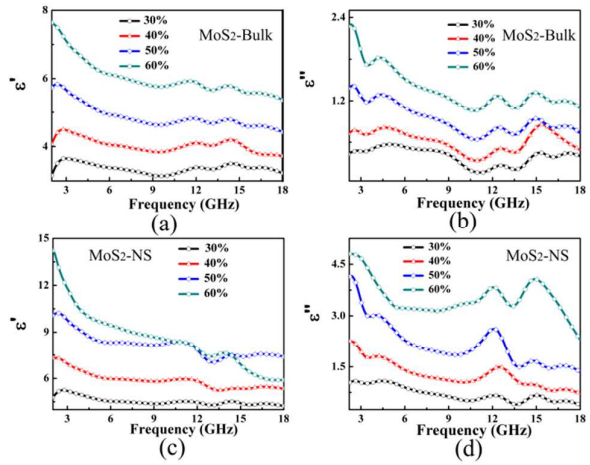


Fig.4 The $\varepsilon'$ of (a) $MoS_2$-Bulk/wax and (c) $MoS_2$-NS/wax with different loadings; $\varepsilon''$ of (b) $MoS_2$-Bulk/wax and (d) $MoS_2$-NS/wax with different loadings.

Dielectric frequency spectra of $MoS_2$-Bulk/wax and $MoS_2$-NS/wax with different loadings (30, 40, 50 and 60 Wt.%) were measured in the frequency range of 2–18 GHz by the coaxial method ( Fig S1). The complex permittivities of $MoS_2$-Bulk/wax are shown in Fig.4 (a-b). The real permittivity ($\varepsilon$') decreases with increasing frequency and increases with increasing loadings. The $\varepsilon$" decreases with increasing frequency firstly, and then appear two relaxation peaks at the frequencies of 12.2 and 15.0 GHz respectively. However, the two relaxation peaks are not very strong. For the $MoS_2$-NS/wax as shown in Fig.4 (c-d), both $\varepsilon$' and $\varepsilon''$ present a similar trend as $MoS_2$-Bulk/wax except that the values of $\varepsilon$' and $\varepsilon$" were almost the double of that of the $MoS_2$-Bulk/wax. Compared with $MoS_2$-Bulk/wax, the relaxation peaks of $MoS_2$-NS/wax become much stronger. It is worth noting that the positions of the relaxation peaks do not change, indicating that the same physical nature of the relaxation for both $MoS_2$-Bulk and $MoS_2$-NS. Generally, the dielectric loss can be expressed by the Debye theory as follows:

$$\varepsilon' = \varepsilon_\infty + \frac{\varepsilon_s - \varepsilon_\infty}{1+\omega^2\tau^2} \qquad (1)$$

$$\varepsilon'' = \frac{\varepsilon_s - \varepsilon_\infty}{1+\omega^2\tau^2}\omega\tau + \frac{\sigma}{\omega\varepsilon_0} \qquad (2)$$

where $\omega$ is the angular frequency, $\tau$ the polarization relaxation time, $\varepsilon_S$ the static permittivity, and $\varepsilon_\infty$ the relative dielectric permittivity at the high frequency limit.

The $\varepsilon'$ decreases with increasing frequency can be explained by Debye theory equation (1)[9,48] and the increasing in $\varepsilon'$ and $\varepsilon''$ with increasing loadings can be interpreted rationally according to the effective medium theory.[49] The equation (2) shows that the $\varepsilon''$ is determined by the polarization and the electrical conductivity ( $\sigma$ ). In general, the relaxations located in the frequency range of 2–18 GHz are caused by the polarization of the defect as reported previously.[13,50-51] According to the first principle calculations and experimental investigations results, $MoS_2$-NS would contain an amount of surface point defects including Vs and $V_{Mo}$[41,52] as illustrated in Figure 5 (a). In $MoS_2$-Bulk samples, the amount of defects is small. For $MoS_2$-NS, more defects would be created by the violent exfoliation process. These point defects would work as dipoles under alternating electric field as illustrated in Figure 5(b). As the relaxation frequency located in the experimental range, the dielectric relaxation peaks could be observed in the dielectric frequency spectra.

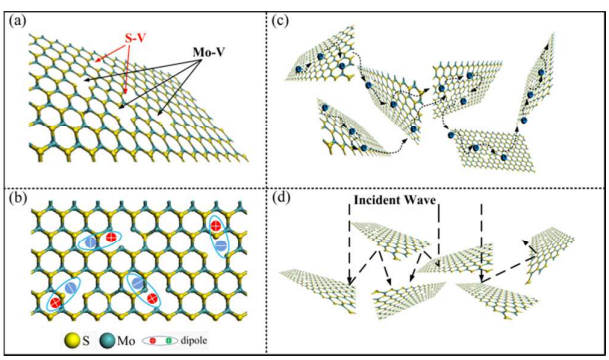


Fig 5. (a) Illustrations of Vs, $V_{Mo}$ defects in single-layer $MoS_2$ (b) dipoles induced by the defect in $MoS_2$-NS/wax (c) Electron transport network of $MoS_2$-NS/wax (d) Microwave propagation model in $MoS_2$-NS/wax

In order to further understand the contribution of the defects in the samples, the $\varepsilon''$ of the annealed $MoS_2$-NS samples is compared with that of the $MoS_2$-Bulk sample as shown in Figure S3. It is found that the $\varepsilon''$ of the annealed $MoS_2$-NS/wax is almost coincident with that of the $MoS_2$-Bulk/wax except for the two relaxation peaks. The intensities of the two relaxation peaks of the annealed $MoS_2$-NS samples are apparently higher than those of $MoS_2$-Bulk samples. That could be ascribed to the existence of a large amount of defects in $MoS_2$-NS samples in spite of the annealing treatment. In addition, $MoS_2$-NS contain a large amount of 1T metallic phase (50% of the total as previous similar reports[31]). The conductivity ( $\sigma$ ) of 1T metallic phase is $10^7$ times higher in magnitude than that of the semiconducting 2H phase. As a result, the high conductivity of $MoS_2$-NS/wax has a positive contribution towards the $\varepsilon''$. Figure S4 (a) shows the $\sigma$ of $MoS_2$-NS/wax with different loadings. For $MoS_2$-Bulk/wax, the conductivity is too small to be measured. The $\sigma$ of $MoS_2$-NS/wax increases slowly from $1.4\times10^{-7}$ to $5.9\times10^{-6}$ $S\cdot m^{-1}$ along with the increasing loading from 30Wt.% to 50Wt.%, while rapidly increases to $2.2\times10^{-5}$ $S\cdot m^{-1}$ when the loading added to 60Wt.%. Figure S4 (b) exhibits the contribution to $\varepsilon''$ from $\sigma$ , which presents an increasing trend with increasing loadings. According to our previous reports,[1,11] the conductive paths could not be built when the loading is relatively low (eg 30, 40Wt.%) and the conductivity loss could be neglected. However, the $MoS_2$-NS/wax with higher loadings (eg 50, 60Wt.%) would have more opportunities to establish conductive paths. When the EM wave propagates into the composites, an amount of electrons of $MoS_2$-NS could migrate along the nanosheets or hop across the defects and the interface as shown in Figure 5 (c) which will make a contribution to the dielectric loss by presenting a higher $\varepsilon''$ value compared to the $MoS_2$-Bulk/wax.

## 3.3. Microwave absorption

In general, the dielectric relaxation enhances the absorption properties of materials. The RL of $MoS_2$-Bulk and $MoS_2$-NS were simulated from the complex permittivity at various thicknesses of the absorber with the following equations:[13]

$$Z_{in} = Z_0(\mu_r/\varepsilon_r)^{1/2}\tanh[j(2\pi fd/c)(\mu_r\varepsilon_r)^{1/2}] \quad (3)$$

$$RL = 20\log\left|(Z_{in}-Z_0)/(Z_{in}+Z_0)\right| \quad (4)$$

where $Z_0$ is the impedance of air, $Z_{in}$ the input impedance of the sample, $c$ the light velocity, $f$ the electromagnetic wave frequency, $d$ the thickness of the absorber, and $\varepsilon_r$ and $\mu_r$ the complex permittivity and permeability of the composite medium.

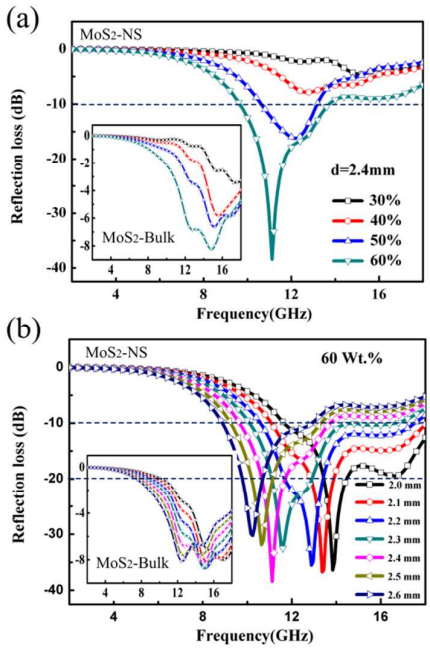


Fig.6 (a) RL of $MoS_2$-Bulk/wax and $MoS_2$-NS/wax with different loadings at the thickness of 2.4 mm. (b) RL of $MoS_2$-Bulk/wax and $MoS_2$-NS/wax with 60 Wt.% at different thicknesses.

Fig.6 (a) shows the RL of the $MoS_2$-Bulk/wax and $MoS_2$-NS/wax with different loadings at the thickness of 2.4mm. It can be found that the RL of $MoS_2$-NS/wax decreases with the increasing loadings. The RL of $MoS_2$-NS/wax with 60 Wt.% loading decreases rapidly to -38.42 dB while that of $MoS_2$-Bulk/wax -8.24 dB under the same condition. Fig.6 (b) shows the RL of the two composites with 60 Wt.% loading at different thickness. The absorption peak of $MoS_2$-NS/wax shifts to lower frequency with the increase of absorber thickness and the optimum thickness is 2.4 mm with a RL of -38.42 dB. In addition, the $MoS_2$-NS/wax with 60 Wt.% loading exhibit a wide bandwidth of effective attenuation (< -10 dB) up to 4.1 GHz ( 9.6-13.76 GHz ). As for $MoS_2$-Bulk/wax, the RL presents a decreasing trend with the increasing thickness and the optimum thickness is 2.6 mm with a RL of -8.73dB. It is worth noting that the RL of the annealed $MoS_2$-NS/wax with 60 Wt.% loading was also calculated at different thickness (Figure S5). The RL shows a similar trend compared with the $MoS_2$-Bulk/wax. However, the maximum absorption of the annealed $MoS_2$-NS/wax composites is at around -22.63 dB which is almost three times of $MoS_2$-Bulk/wax under the same thickness.

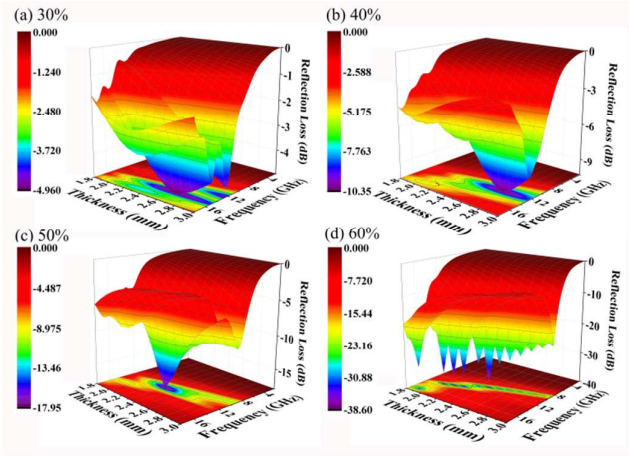


Fig.7 3D plot of the RL versus the frequency and thickness of $MoS_2$-NS/wax

Fig.7 (a-d) show the three dimensional plots of RL of $MoS_2$-NS/wax versus the frequency and thickness at different loadings. The RL of $MoS_2$-NS/wax decreases rapidly from -4.96 dB to -38.60 dB with the increasing loadings while the $MoS_2$-Bulk/wax -3.92 dB to just -8.76 dB as shown in Figure S6. Moreover, as for $MoS_2$-NS/wax with 60% loading, a large absorption bandwidth with RL below -20 dB is observed from 8.48 GHz to 17.84 GHz under the thickness of 1.8-3.0 mm. In order to compare the microwave absorption performance between $MoS_2$-NS and carbon materials, we summarized the corresponding performances in Table S1. It is found that the maximum RL value -38.42 dB of $MoS_2$-NS/wax is higher than all the listed carbon materials except the aligned carbon-nanotube films/PANI which possess a value of -41.14 dB and the effective bandwidth (RL < -10 dB) shows a moderate level among those representative carbon composites. In general, EM attenuation is closely related to the absorptions and multiple internal reflections of electromagnetic waves. Firstly, the dielectric relaxations caused by defects mentioned above have a great contribution to improve the $\varepsilon''$. Secondly, the conductive paths built by the $MoS_2$-NS could transform the

incident wave into heat or other forms of energy, as illustrated in Figure 5(c). Thirdly, the extremely thin and high specific surface areas of $MoS_2$-NS could increase the propagation paths for the incident waves inside the samples compared with $MoS_2$-Bulk as illustrated in Figure 5(d). Those are beneficial to enhance the microwave attenuation performance.

## 4. Conclusions

In summary, we have prepared the $MoS_2$-NS by exfoliation method, and demonstrated the significant enhancement of dielectric properties and microwave absorption performances of $MoS_2$-NS. The $\varepsilon''$ of the $MoS_2$-NS/wax is twice as large as that of the $MoS_2$-Bulk/wax at each loading. The two relaxation peaks observed at the frequencies of 12.2 and 15.0 GHz mainly arise from the defect dipole polarization. Consequently, the $MoS_2$-NS exhibit excellent microwave absorption performance comparable to nanoscale carbon materials. The $MoS_2$-NS/wax has a minimum RL of -38.42 dB at the thickness of 2.4 mm and the effective absorption bandwidth (< -10 dB) up to 4.1 GHz. It is believed that the $MoS_2$-NS is a promising candidate in microwave absorption application and we anticipate that our work could be extended to other LTMD.

## Acknowledgements

This work is supported by the National Natural Science Foundation of China under Grant No. 50972015, 51132002, and 51172026.

## Notes and references


1 B. Wen, M. S. Cao, M. M. Lu, W. Q. Cao, H. L. Shi, J. Liu, X. X. Wang, H. B. Jin, X. Y. Fang,W. Z. Wang and J.Yuan, *Adv. Mater*, 2014, 26, 3484.
2 R. C. Che, L. M. Peng, X. F. Duan, Q. Chen and X. L. Liang, *Adv. Mater*, 2004, 16, 401.
3 J. W. Liu, R. C. Che, H. J. Chen, F. Zhang, F. Xia, Q. S. Wu and M. Wang, *Small*, 2012, 8, 1214.
4 Z. J. Wang, L. Wu, J. G. Zhou, Z. H. Jiang and B .Z. Shen, *nanoscale,2014,6,12298.*
5 H. J. Yang,M. S. Cao, Y. Li,H. L. Shi, Z. L. Hou, X. Y. Fang,H. B. Jin, W. Z. Wang and J. Yuan, *Adv. Opt. Mater*, 2014, 2, 214
6 M. S. Cao, J. Yang, W. L. Song, D. Q. Zhang, B. Wen, H. B. Jin, Z. L. Hou and J. Yuan, *ACS Appl. Mater. Interfaces*, 2012, 4, 6949
7 T. Xia, C. Zhang, N. A. Oyler and X. B. Chen, *Adv. Mater*, 2013, 25, 6905.
8 M. Mahmoodi, M. Arjmand, U. Sundararaj and S. Park, *Carbon*, 2012, 50, 1455.
9 B. Wen, M. S. Cao, Z. L. Hou, W. L. Song, L. Zhang, M. M. Lu, H. B. Jin, X. Y. Fang, W. Z. Wang and J. Yuan, *Carbon*, 2013, 65, 124.
10 P. C. P. Watts, W. K. Hsu, A. Barnes and B. Chambers, *Adv. Mater,* 2003, 15, 600.
11 W. L. Song, M. S. Cao, M. M. Lu, J. Liu, J. Yuan and L. Z. Fan, *J. Mater. Chem. C*., 2013, 1, 1846.
12 H.Sun , R.C.Che ,X.You , Y.S. Jiang , Z.B. Yang , J. Deng , L.B Qiu ,and H.S. Peng, *Adv. Mater*. 2014, 26, 8120
13 N.J Tang,W. Zhong, C.T. Au,Y. Yang, M,G Han,K.J Lin and Y. W Du, *J. Phys. Chem. C*, 2008, 112, 19316.
14 G. Li, T.S.Xie, S.L. Yang, J.H. Jin, and J.M. Jiang, *J. Phys. Chem. C* ,2012, 116, 9196.
15 B. Wen, X. X. Wang, W. Q. Cao, H. L. Shi, M. M. Lu, G. Wang, H. B. Jin, W. Z. Wang, J. Yuan and M. S. Cao, *Nanoscale*, 2014, 6,5754.
16 R. Lv, Q. Li, A. R. Botello-Mendez, T. Hayashi, B. Wang, A. Berkdemir, Q. Hao, A. L. Elias, R. Cruz-Silva, H. R. Gutierrez, Y. A. Kim, H. Muramatsu, J. Zhu, M. Endo, H. Terrones, J. C. Charlier, M. Pan, and M. Terrones, *Sci. Rep,* 2012, 2, 586.
17 G.K. Lim, Z.L. Chen, J. Clark, R.G.S. Goh, W.H. Ng, H.W. Tan, R.H. Friend, P.K.H. Ho and L.L. Chua, *Nature Photonics,* 2011, 5, 554.
18 Q. L.Bao, H. Zhang, Y. Wang, Z.H Ni, Y. L.Yan, Z.X. Shen, K.P. Loh and D.Y. Tang, *Adv. Funct. Mater,* 2009, 19, 3077.
19 Z. Liu, L.L. Ma, G. Shi, W. Zhou, Y.J. Gong, S. D.Lei, X.B. Yang, J. Zhang, J. N.Yu, K.P. Hackenberg, A. Babakhani, J.C. Idrobo, R. Vajtai, J. Lou and P.M. Ajayan, *Nature nanotechnology,* 2013, 8, 119.
20 I. Jo, M.T. Pettes, J. Kim, K. Watanabe, T. Taniguchi, Z. Yao and L. Shi, *Nano Lett,* 2013, 13 , 550.
21 P. Niu, L.L. Zhang, G. Liu and H.M. Cheng, *Adv. Funct. Mater,* 2012, 22, 4763.
22 X. D. Zhang, X. Xie, H. Wang, J.J. Zhang, B.C. Pan and Y. Xie, *J. Am. Chem. Soc*, 2013, 135, 18.
23 Y. D. Hou, A.B. Laursen, J. S. Zhang, G. G. Zhang, Y. S. Zhu, X. C. Wang, S. Dahl and I. Chorkendorff, *Angew. Chem. Int. Ed. Engl,* 2013, 52, 3621.
24 M. Chhowalla, H.S. Shin, G. Eda, L.J. Li, K.P. Loh and H. Zhang, *Nature chem*, 2013, 5, 263.
25 X. Huang, Z.Y. Zeng and H. Zhang, *Chem.Soc.Rev*, 2013, 42, 1934.
26 H.Li, J. Wu, X. Huang, G. Lu, J. Yang, X. Lu, Q.H.Xiong and H. Zhang, *ACS Nano*, 2013, 11, 10344.
27 M. S. Xu, T. Liang, M.M. Shi, and H.Z. *Chen, Chem. Rev*.,2013,113, 3766.
28 M. Chhowalla1, H. S. Shin, G. Eda, L.J. Li, K.P. Loh and H. Zhang, *NATURE CHEMISTRY*,2013,5,263
29 S.Hu and X.Wang, *Chem. Soc. Rev*, 2013,42, 5577.
30 A. Splendiani, L. Sun, Y. B. Zhang, T. S. Li, J. Kim, C.Y. Chim, G. Galli and F. Wang, *Nano Lett*, 2010, 10, 1271.
31 G. Eda, H. Yamaguchi, D. Voiry, T. Fujita, M. Chen and M. Chhowalla, *Nano Lett*, 2011, 11, 5111.
32 J.D. Benck, Z. B. Chen, L.Y. Kuritzky, A.J. Forman and T.F. Jaramillo, *ACS Catalysis*, 2012, 2, 1916.
33 D. Voiry, M. Salehi, R. Silva, T. Fujita, M. W. Chen, T. Asefa, V.B. Shenoy, G. Eda and M. Chhowalla, *Nano Lett*, 2013, 13, 6222.
34 A.B. Laursen, S. Kegnæs, S. Dahl and I. Chorkendorff, *Energy & Environmental Science*, 2012, 5 5577.
35 G. Cunningham, M. Lotya, C.S. Cucinotta, S. Sanvito, S. D. Bergin, R.t Menzel, M.S. P. Shaffer and J. N. Coleman, *ACS Nano*, 2012, 6, 3468.
36 P. Joensen, R.F. Frindt and S.R. Morrison, *Mater. Res. Bull*, 1986, 21, 457.

37 R. A. Gordon, D. Yang, E. D. Crozier, D. T. Jiang and R. F. Frindt, *Physical Review B*, 2002, 65, 125407.
38 D. Yang, S. J. Sandoval, W. M. R. Divigalpitiya, J. C. Irwin and R. F. Frindt, *Physical Review B*, 1991, 43, 12053.
39 F. Wypych and R. Schollhorn, J. Chem. *Soc. Chem. Commun*,1992, 1386.
40 S. KC, R. C Longo, R. Addou, R. M. Wallace and K. Cho, *Nanotechnology* , 2014,25, 375703.
41 W. Zhou, X.L. Zou, S. Najmaei, Z. Liu, Y.M. Shi, J.Kong, J. Lou, P. M. Ajayan, B. I. Yakobson, and J.C. Idrobo, *Nano Lett*, 2013, 13, 2615.
42 H.P.Komsa, S.Kurasch, O. Lehtinen, U. Kaiser, and A.V. Krasheninnikov, *PHYSICAL REVIEW B*, 2013, 88, 035301.
43 W. L. Song, M. S. Cao, B. Wen, Z. L. Hou, J. Cheng, and J. Yuan, *Mater.Res.Bull*, 2012, 47, 1747
44 C. G. Lee, H. Yan, L. E. Brus, T. F. Heinz, J. Hone, and S.Ryu, *ACS Nano*,2010, 4, 2695.
45 H. S. S. R.Matte, A. Gomathi, A. K. Manna, D. J. Late, R.Datta, S.K. Pati, and C. N. R. Rao, *Angew. Chem*. 2010, 122, 4153.
46 F. Wypych and R.Schollhorn, *J. Chem. Soc.Chem.Commun*,1992, 1386.
47 S. S. Chou,Y. K. Huang, J. Kim, B. Kaehr, B. M. Foley, P. Lu, C. Dykstra, P. E. Hopkins, C. J Brinker, J. X. Huang, and V.P. Dravid, *J. Am. Chem. Soc*. 2015, 137, 1742.
48 W. L. Song, M. S. Cao, B. B. Qiao, Z. L. Hou, M. M. Lu, C. Y. Wang, J. Yuan, D. N. Liu, and L. Z. Fan, *Mater.Res.Bull*, 2014, 51, 277.
49 J. V. Mantese, A. L.Micheli, D. F. Dungan, R. G. Geyer, J. B. Jarvis, and J. Grosvenor, *J.Appl.Phys*, 1996, 79, 1655.
50 H.L. Zhu, Y.J. Bai, R. Liu, N. Lun, Y.X. Qi, F.D. Han and J.Q. Bi, *J. Mater. Chem*, 2011, 21, 13581.
51 B. S. Meng and B. D. B. Klein, *PHYSICAL REVIEW B.*,1996,53,12777.
52 S. K.C, R. C. Longo, R. Addou, R. M. Wallace and K. Cho, *Nanotechnology*,2014,25,375703.